Infrared Phys. Vol. 34, No. 2, pp. 175–189, 1993
Printed in Great Britain.

0020-0891/93 $6.00 + 0.00

A NEW MULTI-CHANNEL HETERODYNE POLARIMETER FOR PLASMA CURRENT AND ELECTRON DENSITY MEASUREMENTS

JOHN HOWARD

Plasma Research Laboratory, Research School of Physical Sciences and Engineering, Australian National University, Canberra, A.C.T., Australia

(Received for publication 4 November 1992)

Abstract—A spatially-scanning phase-sensitive heterodyne far-infrared (FIR) polarimeter/interferometer for measurement of plasma current and electron densities is described. The instrument utilizes a rotating diffraction grating wheel for the dual purpose of spatially scanning the plasma cross section and providing a Doppler frequency offset for heterodyne detection purposes. Only two detectors are required to obtain accurate interferometric and polarimetric information for 15 discrete spatial chords. A novel approach to the optical processing of the initially linearly polarized probe beam allows the Faraday rotation of the vibrational ellipse to be unambiguously encoded as a phase modulation on the intermediate frequency carrier signals extracted from the two detectors. The plasma birefringence can be recovered from the corresponding amplitude modulation.

1. INTRODUCTION

The anisotropic nature of the dielectric tensor for a plasma embedded in a magnetic field results in significant changes to the polarization state of a probing electromagnetic wave.[1–4] In particular, for a linearly polarized beam of vacuum wavelength λ_0 (typically infrared to far-infrared) propagating in ordinary mode in the plasma, the wave electric vector suffers a rotation given by:[4]

$$\psi \approx 2.6 \times 10^{-13} \lambda_0^2 \int_0^L n_e B_\parallel \, \mathrm{d}l \tag{1}$$

where $B_\parallel = \mathbf{B} \cdot \widehat{\mathrm{d}\mathbf{l}}$, $\mathbf{B}$ is the magnetic field, $\widehat{\mathrm{d}\mathbf{l}}$ is the unit vector in the propagation direction, n_e is the electron density, $\mathrm{d}l$ is a line element and SI units are used. The rotation is caused by the slightly different phase velocities for the circularly polarized characteristic wave modes (circular birefringence). For n_e known, measurements of ψ at many viewing chords in a poloidal plane can be used to infer approximately the toroidal current density distribution in tokamak plasmas.[3] Measurement of the Faraday rotation angle in the midplane of larger tokamak devices can also be used for plasma densitometry, with potentially significant advantages over standard interferrometric techniques that measure the line integral of the electron density.[1,5] An accurate measure of the rotation angle would also be a useful adjunct to interferometry of stellarator plasmas, where (at least for low plasma pressure) the confining magnetic field is well known.

Most measurements of ψ have been plagued by uncertainties related to the difficulty of measuring the typically quite small angular rotations. In particular, the existence of a transverse magnetic field component causes a phase difference between the wave electric field components parallel and perpendicular to the transverse magnetic field[4]

$$\phi = 1.2 \times 10^{-18} \lambda_0^3 \int_0^L n_e |\mathbf{B} \times \widehat{\mathrm{d}\mathbf{l}}|^2 \, \mathrm{d}l. \tag{2}$$

(Note that the angles ψ and ϕ are doubled for a double traversal of the plasma.) The linear birefringence induced phase shift ϕ can interfere with accurate measurement of ψ. Given the different scalings it is possible to choose λ_0 such that ϕ can be neglected compared with ψ.[4]

Invariably, however, ψ is then itself small, requiring elaborate techniques for its accurate measurement. Extraction of current density information from the measured Faraday rotation profile is therefore extremely noise prone, depending as it does on reliable knowledge of the electron density distribution and accurate measurements of ψ along many chords and in many directions.

The most straightforward approach for determination of ψ is to measure the power transmitted through an analyzer aligned to reject the unperturbed beam.[6] This method is complicated by analyzer leakage, the effects of refraction and beam ellipticity. Dodel and Kunz[7] (and independently, Erickson *et al.*)[8] proposed the determination of the Faraday angle by passing two spatially superimposed frequency offset circularly polarized beams through the plasma and measuring the phase difference 2ψ using frequency-shift heterodyne techniques. The method is insensitive to beam ellipticity and laser power fluctuations and robust against common-mode refractive effects. Being a phase sensitive technique it should also enjoy the usual signal-to-noise advantages over amplitude encoding methods.[9] However, it is experimentally quite cumbersome to generate the required rotating linearly polarized input beam.[10,8] Some variants of these schemes, most notably the rocking polarization method[11] and the rotating polarization ellipse technique[12] have also been implemented. Through 15 chordal channels with angle resolution $\leqslant 0.2^\circ$ have been obtained in the latter case, the frequency response is limited by mechanical modulation methods to ~ 1 kHz. All approaches suffer from the usual technical difficulties associated with furnishing sufficient viewing chords for reasonable information retrieval.

In this paper we address the dual problem of sufficient spatial sampling of the plasma and adequate rotation angle resolution without prohibitive cost or optical system complexity. We report the construction and operation of a 15 channel heterodyne polarimeter/interferometer designed to measure the interferometric phase, the Faraday rotation ψ and birefringence phase shift ϕ. The polarimeter uses a new method for ellipsometric analysis of the probe beam polarization where the ellipse tilt angle ψ is encoded as a phase difference 2ψ between orthogonal carriers. Many spatial channels of information are obtained by multiplexing the chordal information in either the time or frequency domains, allowing the use of a common optical path and thus a single set of optics and only two detecting elements.

The polarimeter described here features several unique advantages over conventional phase sensitive systems. First, only a linearly polarized input beam is required: there is no need for frequency shifting and superposition of orthogonal circularly polarized waves. This avoids the problems associated with wavefront and power matching of the independent beams. There is also no requirement for mechanical or optical modulation of the incident wave polarization. The transformation of the polarization ellipse tilt angle into a time-domain phase modulation of the detector signals is achieved using a few simple post-processing optical elements. Only two detectors are required to monitor this relative phase shift between orthogonal components of the probing electric field vector. It will be shown that when the ellipse rotation angle is small, it is possible to amplify optically the phase angle 2ψ though at some possible cost in angle signal-to-noise, depending on the noise source.

Multiple spatial channels are obtained using a rotating grating wheel that both frequency shifts (for heterodyne detection) and sweeps the beam (by means of an angularly dependent grating constant) through a modest range of diffraction angles in the plane of incidence.[13] The signals from different spatial channels are thus multiplexed in the time domain. On execution of a double pass of the plasma the diffracted beams are, in time sequence, returned by the grating along their incident path and sampled by a beamsplitter. (Another approach, where the information is multiplexed in the temporal frequency domain,[14] will be discussed elsewhere.) The resulting economy of optical elements is of great practical advantage and can be important when access is limited. The wheel has been rotated at speeds up to 200 s^{-1} using an air turbine drive[13] to produce double pass Doppler shifts greater than 750 kHz. By multi-partitioning the wheel, it is possible to achieve plasma scan rates approaching 1 kHz with polarimetric phase angle resolution of $\leqslant 0.1^\circ$.

The interferometric phase shift, which is common to each polarimeter channel, can be extracted (with correction for the Faraday phase angle) by comparing with a signal derived by optically monitoring the grating groove frequency or from the intermediate frequency (IF) signal yielded by a separate reference interferometer.

The theory for the polarimeter is developed using the Jones matrix formalism in Section II. A far-infrared (FIR) polarimeter designed to check the theory is described in Section III. A new computational method is used to demodulate the digitized raw signals to extract the quantities 2ψ and ϕ. A factor of 10 advantage in angular resolution is obtained by the phase modulation technique over the usual amplitude encoding. Measurements confirming the polarimeter behaviour are reported in Section IV. Finally, an analysis of non-ideal optical effects that influence the instrument response are given in the Appendix.

II. THEORETICAL DESCRIPTION

We assume that the polarimeter system is fed by a linearly polarized laser beam ($\omega_0 = 2\pi c/\lambda_0$) having electric vector initially aligned along the x-axis. For consistency with the experimental arrangement we take the x axis in the vertical direction as shown in Fig. 2. The incident electric vector can be expressed as the real part of

$$\mathbf{E}_0 = \exp(j\omega_0 t)\begin{pmatrix}1\\0\end{pmatrix}. \tag{3}$$

As shown in Fig. 5, apart from reflection losses and Doppler shifting by the rotating grating, the initial linearly polarized beam is preserved up to entry of the plasma. Assuming the return mirror to be ideal, and provided the magnetic field component transverse to the beam is aligned with respect to the coordinate system, the field emerging from the plasma can be expressed as

$$\mathbf{E} = \exp[j(\omega_0 + \Omega)t]\begin{pmatrix}1\\ \tan\eta\ \exp(j\phi)\end{pmatrix} \tag{4}$$

where $\tan\eta$ is ratio of the component amplitudes and ϕ is the birefringence induced phase shift given by equation (2). The field can also be written in terms of the Faraday angle ψ, i.e. the inclination of the major axis of the polarization ellipse to the x axis (see Fig. 1), and the ellipticity $\tan\chi$, the ratio of the minor and major axes of the ellipse, by

$$\mathbf{E} = A\ \exp[j(\omega_0 + \Omega)t]\mathbf{R}_\psi\begin{pmatrix}1\\ \pm j\tan\chi\end{pmatrix} \tag{5}$$

where $\mathbf{R}_\psi$ is the matrix for coordinate rotation by ψ and A is an amplitude factor. Comparing equations (4) and (5) it can be shown that the ellipse quantities are related by

$$\tan 2\psi = \tan 2\eta \cos\phi \tag{6}$$

$$\sin 2\chi = \sin 2\eta \sin\phi. \tag{7}$$

These angles will prove to be useful for the Jones matrix analysis of the optical system that follows. It is convenient, however, to describe the evolution of the polarization state of the probe wave in the plasma in terms of its Stokes parameters, the cartesian coordinates $\mathbf{s} = (s_1, s_2, s_3)$ of the point on the Poincare sphere representing the polarization state (ψ, χ):

$$\begin{aligned} s_1 &= \cos 2\chi \cos 2\psi \\ s_2 &= \cos 2\chi \sin 2\psi \\ s_3 &= \sin 2\chi. \end{aligned} \tag{8}$$

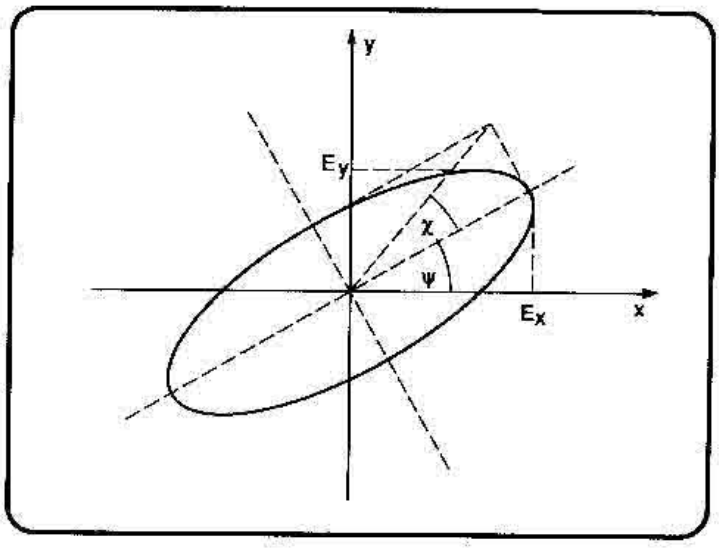

Fig. 1. Schematic diagram of the rotational ellipse showing rotation and ellipticity and the component amplitudes E_x and E_y.

A series expansion solution for the evolution of the probe beam polarization on passage through the plasma[1,3] allows the Stokes parameters to be directly related to physical quantities of interest. In particular, for tokamak poloidal field measurements (B_T in the y direction, propagation in the z direction) with initial polarization $\mathbf{s}_0 = (1, 0, 0)$ the final polarization state is given by $\mathbf{s}_P \approx (1, s_{2P}, 0)$ where, for beam frequencies much greater than the plasma and cyclotron frequencies, and provided the total phase change between the characteristic waves is small, s_{2P} is given by the r.h.s. of equation (1). The beam ellipticity (due to the linear birefringence phase shift ϕ) appears when higher order terms in the series expansion solution for the evolution of $\mathbf{s}$ are retained.

Figure 2 shows a detailed view of the processing optics (for now ignoring the grating and beamsplitter) required to generate the independent polarimetric signals from the return beam **E**. The local oscillator (LO), derived from the incident laser beam and polarized in the y direction, is combined with the return radiation at the free-standing wire-grid polarizer P1. The wires of P1 are oriented at 45° to the x-axis so that the LO and probe beams incident on the detectors (which

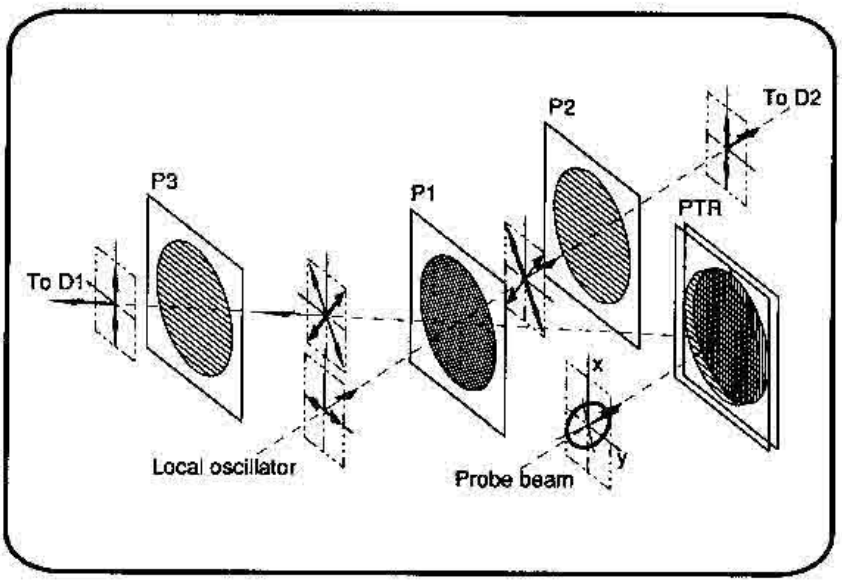

Fig. 2. Schematic diagram of the optical arrangement required for polarization analysis of the return probe beam from the plasma. Thick lines are used to show the electric vector for the probe beam and thin for the local oscillator beam.

The interferometric phase shift, which is common to each polarimeter channel, can be extracted (with correction for the Faraday phase angle) by comparing with a signal derived by optically monitoring the grating groove frequency or from the intermediate frequency (IF) signal yielded by a separate reference interferometer.

The theory for the polarimeter is developed using the Jones matrix formalism in Section II. A far-infrared (FIR) polarimeter designed to check the theory is described in Section III. A new computational method is used to demodulate the digitized raw signals to extract the quantities 2ψ and ϕ. A factor of 10 advantage in angular resolution is obtained by the phase modulation technique over the usual amplitude encoding. Measurements confirming the polarimeter behaviour are reported in Section IV. Finally, an analysis of non-ideal optical effects that influence the instrument response are given in the Appendix.

II. THEORETICAL DESCRIPTION

We assume that the polarimeter system is fed by a linearly polarized laser beam ($\omega_0 = 2\pi c/\lambda_0$) having electric vector initially aligned along the x-axis. For consistency with the experimental arrangement we take the x axis in the vertical direction as shown in Fig. 2. The incident electric vector can be expressed as the real part of

$$\mathbf{E}_0 = \exp(j\omega_0 t)\begin{pmatrix}1\\0\end{pmatrix}. \tag{3}$$

As shown in Fig. 5, apart from reflection losses and Doppler shifting by the rotating grating, the initial linearly polarized beam is preserved up to entry of the plasma. Assuming the return mirror to be ideal, and provided the magnetic field component transverse to the beam is aligned with respect to the coordinate system, the field emerging from the plasma can be expressed as

$$\mathbf{E} = \exp[j(\omega_0 + \Omega)t]\begin{pmatrix}1\\ \tan\eta\ \exp(j\phi)\end{pmatrix} \tag{4}$$

where $\tan\eta$ is ratio of the component amplitudes and ϕ is the birefringence induced phase shift given by equation (2). The field can also be written in terms of the Faraday angle ψ, i.e. the inclination of the major axis of the polarization ellipse to the x axis (see Fig. 1), and the ellipticity $\tan\chi$, the ratio of the minor and major axes of the ellipse, by

$$\mathbf{E} = A\ \exp[j(\omega_0 + \Omega)t]\mathbf{R}_\psi\begin{pmatrix}1\\ \pm j\tan\chi\end{pmatrix} \tag{5}$$

where $\mathbf{R}_\psi$ is the matrix for coordinate rotation by ψ and A is an amplitude factor. Comparing equations (4) and (5) it can be shown that the ellipse quantities are related by

$$\tan 2\psi = \tan 2\eta \cos\phi \tag{6}$$

$$\sin 2\chi = \sin 2\eta \sin\phi. \tag{7}$$

These angles will prove to be useful for the Jones matrix analysis of the optical system that follows. It is convenient, however, to describe the evolution of the polarization state of the probe wave in the plasma in terms of its Stokes parameters, the cartesian coordinates $\mathbf{s} = (s_1, s_2, s_3)$ of the point on the Poincare sphere representing the polarization state (ψ, χ):

$$\begin{aligned} s_1 &= \cos 2\chi \cos 2\psi \\ s_2 &= \cos 2\chi \sin 2\psi \\ s_3 &= \sin 2\chi. \end{aligned} \tag{8}$$

From now on g is called the optical gain and $\phi_0 = \gamma + \delta$ is the total optical phase shift between the orthogonal components of E.

Mixing E_1 and E_2 with the local oscillator at frequency ω_0 results in IF carriers at 2Ω at the output ports of detectors D1 and D2. These carriers can be demodulated using digital methods or electronic phase detectors to recover unambiguously the instantaneous phase difference Q and relative amplitude R to bandwidth 2Ω. In practice, we must also allow for a constant phase offset Q_0 and accommodate the relative detector sensitivities through a scale factor R_0. The phase offset is due both to polarizer leakage (see Appendix) and possible alignment inaccuracies that allow the detectors to sample slightly different portions of the mixed probe and local oscillator beams.

1. Phase difference and amplitude ratio

Defining the phase difference $Q = \phi_1 - \phi_2$, it is easily shown using equations (13) and (14) that

$$\tan Q = \sin(\phi + \phi_0)\tan 2\eta' \tag{15}$$

$$\tan \eta' = g \tan \eta \tag{16}$$

and that the ratio of the signal amplitudes $R = |E_1|/|E_2|$ is given by

$$R = \frac{1 + \tan^2 \eta' - 2 \tan \eta' \cos(\phi + \phi_0)}{1 + \tan^2 \eta' + 2 \tan \eta' \cos(\phi + \phi_0)}. \tag{17}$$

For unit optical gain $g = 1$, $\tan \eta'$ is identical to $\tan \eta$ the ratio of the ellipse component amplitudes. When the optical phase is adjusted so that $\phi_0 = 90°$, and setting $g = 1$, we obtain the important result

$$\tan Q = \tan 2\eta \cos \phi \equiv \tan 2\psi = \frac{s_2}{s_1} \tag{18}$$

so that, for poloidal field measurements, $\tan Q$ is a measure of the line integral quantity s_{2P} (since $s_{1P} \approx 1$). For the amplitude ratio we obtain

$$\frac{1 - R}{1 + R} = \sin 2\eta \sin \phi = \sin 2\chi = s_3 \tag{19}$$

so that R measures the ellipticity caused by the plasma birefringence.

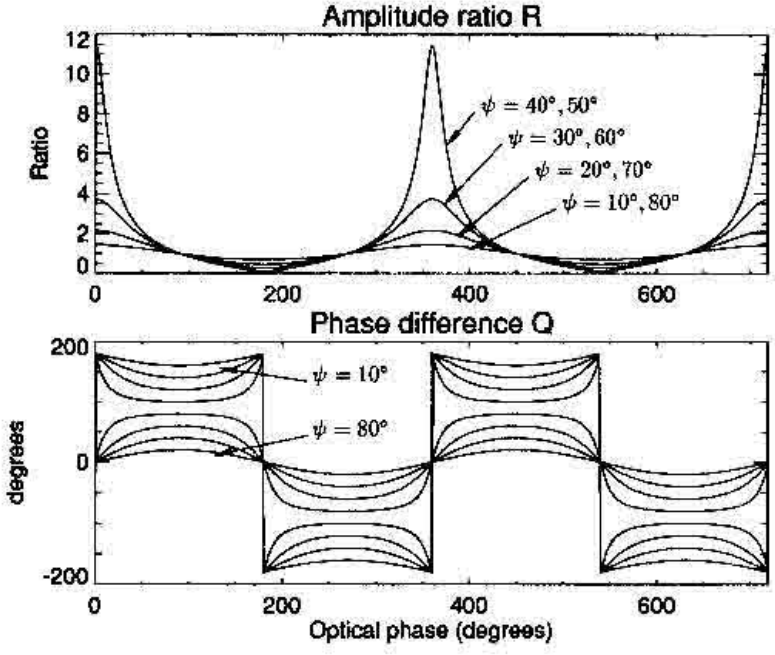

Fig. 3. Dependence of the phase difference Q and the amplitude ratio R on the optical phase ϕ_0 for various values of the ellipse tile angle ψ.

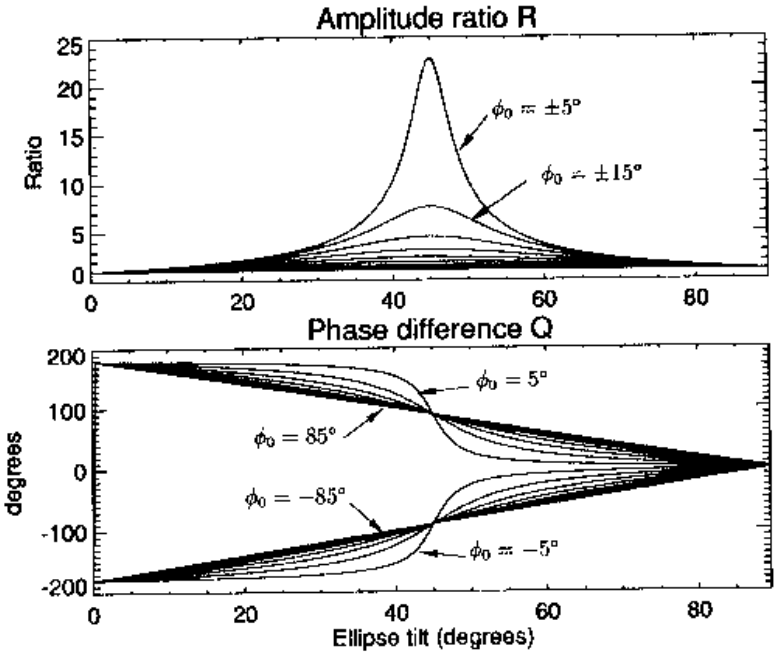

Fig. 4. Dependence of the amplitude ratio R and the phase difference Q on the ellipse tilt angle ψ for values of the optical phase $\phi_0 = -85°$ (10°) 85°. Note that Q is proportional to ψ when $\phi_0 = 0$.

When $\phi_0 = 0$ (the standard case) the phase difference Q depends on both the ellipse tilt and the birefringence

$$\tan Q = \tan 2\eta \sin \phi = \frac{s_3}{s_1} \tag{20}$$

while the amplitude ratio gives s_2 (but a birefringence-contaminated measure of ψ):

$$\frac{1 - R}{1 + R} = \sin 2\eta \cos \phi = s_2. \tag{21}$$

In bench experiments we can exercise control directly over the tilt ψ and phase shift ϕ and so examine these parameter dependences for Q and R. The variation of Q and R with ϕ_0 for $g = 1$ and ellipse tilt angles between 10° and 80° is shown in Fig. 3. Note the quadrature behaviour of the phase and amplitude to the tilt angle ψ. These curves can become somewhat distorted when the polarizer leakage is significant (see Appendix).

The dependence of Q and R on the ellipse tilt ψ for $g = 1$ and values of ϕ_0 spanning 0° to 180° is illustrated in Fig. 4. The relationship between Q and ψ remains approximately linear for values of ϕ_0 within $\pm 20°$ of $\phi_0 = 90°$. As expected, Q becomes independent of ψ as the phase offset ϕ_0 tends to zero.

When $g \neq 1$, the relationship between Q and ψ is dependent on the birefringence. However, in the important special case where ϕ is small (as is true for sufficiently small probing wavelength), this correction enters only in second order. The exact dependence is obtained by casting equation (15) (for $\phi_0 = \pi/2$) in terms of the Faraday angle ψ and birefringence ϕ:

$$\tan Q = \frac{2g \tan 2\psi \cos \phi}{(1 + g^2)\cos \phi + (1 - g^2)(\cos^2 \phi + \tan^2 2\psi)^{1/2}}. \tag{22}$$

In the regime where ϕ is small, the Faraday angle is likely also to be small, and it is possible to make use of the optical gain factor g to give significant phase angle enhancement. Physically, this arises when the optical transmission for the rotated component is greater than for the incident wave. With $\cos \phi \approx 1$ and $\tan 2\psi \approx 2\psi$ we have $\eta \approx \psi$. Equations (15) and (16) then yield $Q = 2g\eta \approx 2g\psi$ valid to third order in $g\psi$. However, as noted by Erikson *et al.*,[8] such enhancements are valuable only in as much as the angle signal-to-noise ratio is also improved.

III. EXPERIMENT

The layout of the single-view scanning polarimeter is shown in Fig. 5. An HCN laser ($\lambda_0 = 337\ \mu$m) provides a 10 mW Gaussian beam linearly polarized at $\sim 45°$ to the vertical (the x direction). The first polarizer ($\alpha = 90°$) transmits the vertically polarized probe beam and reflects the horizontal component to act as LO for detectors D1 and D2. The probe beam is partially reflected by the Mylar beamsplitter and expanded before focusing onto the grating wheel circumference (wheel radius 150 mm) at an incidence angle of 30°. The multi-sectored blazed grating sequentially diffracts the beam into a fan array of 15 beams clustered within an angle of 20° about the grating normal. A cylindrical polyethylene lens is used to correct for the asymmetric grating reflectivity and a curved cylindrical mirror reflects the diffracted beams to the grating for return along the incident path. The return beams transmitted by the Mylar splitter are then analyzed in turn by the polarimetric optics as described in the previous section. Since the beamsplitter has greater transmission for the horizontal component, and because of the better grating reflection efficiency for $\mathbf{E}_0$ perpendicular to the grooves, the incident beam is chosen to be vertically polarized (parallel to the grating grooves) in order that there be a net optical gain $g > 1$.

Among the many advantages of the configuration are the relatively simple layout requiring minimal alignment and maintenance. The grating serves to disperse and recombine the beams while the associated plasma double pass doubles the measurable Faraday phase shift. Also, the system is almost totally immune to extraneous vibration-induced phase noise, these effects being common to both detectors. The only source of noise is possible variations in the PTR mirror-polarizer separation δ. When ϕ is small, this error should enter only in second order. To minimize this movement, the mirror and polarizer are physically linked. Their separation is adjusted by a precision micrometer thread machined on the outer circumference of the 90 mm diameter polished brass mirror insert that mates with the polarizer mounting. Clearly, a birefringent quartz plate of the appropriate phase delay δ would eliminate this noise source.

The main limitations of the Michelson arrangement are the susceptibility of the laser to feedback modulation by return beams from the Mylar splitter and corner-cube Schottky diode detectors, and crosstalk (via the grating) between the detectors that must be polarization isolated as shown in

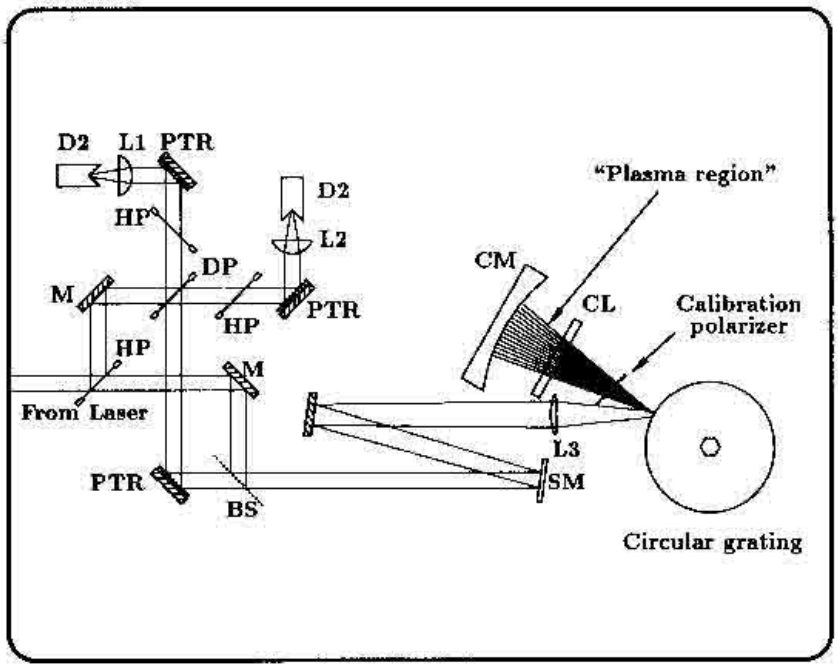

Fig. 5. Schematic diagram of the scanning polarimeter layout. Key: BS—beam splitter, CL—cylindrical lens, CM—cylindrical mirror, D1, D2—Schottky diode detectors, DP—45° polarizer, L1 and L2—f = 10 cm lenses, L3—f = 26 cm lens, M—plane mirror, SM—f = −140 cm spherical mirror, VP—vertical polarizer. The inset is a close view of the groove shape at the position of the incident beam.

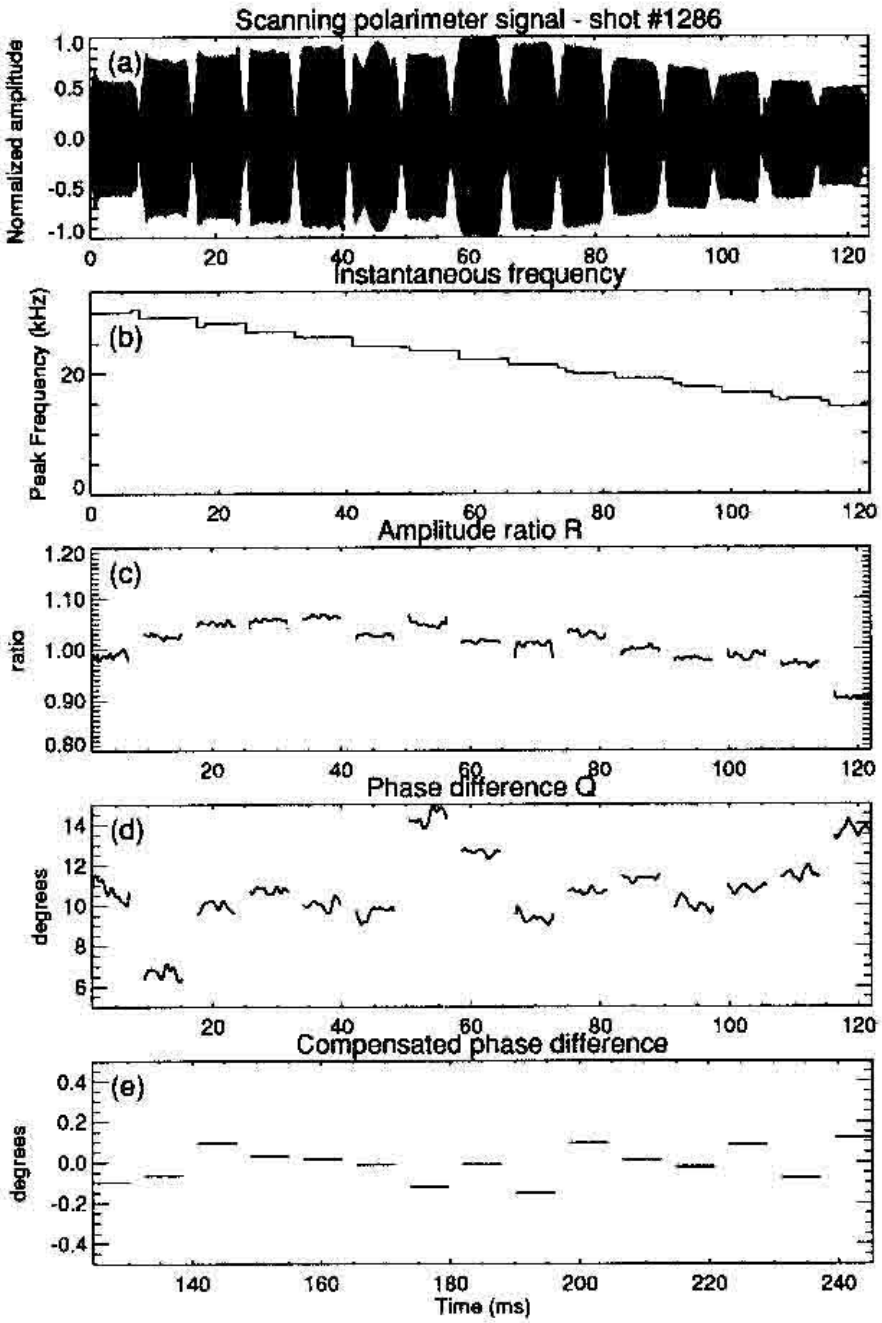

Fig. 6. (a) Interference fringes produced by the scanning polarimeter at detector D1. (b) Time evolution of the fringe frequency. Beams diffracted at different angles suffer different Doppler offsets. (c) The ratio R of the signal envelopes at detectors D1 and D2. (d) Phase difference Q between detectors D1 and D2. (e) Average phase shift during the next wheel revolution after subtraction of the baseline phase profile shown in (d).

Fig. 5. The level of laser feedback modulation from the Mylar splitter can be checked by blocking the return beam following the compensating PTR. The crosstalk due to imperfect isolation of the detectors is monitored by blocking the probe beam after the first horizontal polarizer. These effects, which can cause phase distortion of the IF carriers can be reduced by the use of appropriate attenuators.

1. Signal processing and demodulation

The temporal sequence of fringe bursts from detector D1 for $\psi = 0$ are shown in Fig. 6(a). The corresponding time-dependent fringe frequency calculated from the peak of the power spectrum

in a moving time window of width 1.2 ms is shown in Fig. 6(b). The Doppler offset for the separate fringe bursts changes with diffraction angle. The detector alignment can be adjusted so that the relative amplitudes of the bursts obtained at D1 and D2 vary by less than $\sim 10\%$ across the 15 channels [Fig. 6(c)]. For the measurements presented here, the grating typically rotates at approx. 20 Hz, thereby effecting a scan every 50 ms with $\tau_d \sim 3$ ms dwell of the probe beam at each scan position (equi-angular sectors).

A numerical demodulation algorithm applied to the signals from D1 and D2 is used to compute the phase difference Q and amplitude ratio R. To minimize possible channel crosstalk at the transition times between adjacent fringe bursts, only the central portion $\tau_p = \zeta\tau_d$, $\zeta = 0.7$ of a given burst is processed. The carrier and its sidebands are bandpass filtered to reduce noise. The minimum filter bandwidth is equal to the inverse of the processed time interval $f_p = 1/\tau_p$ corresponding to a fixed number of interference fringes $KV\tau_p/2\pi$ for each probe beam. The negative frequency components of the Fourier transformed time series are then set to zero before inverse Fourier transformation to yield the complex time domain analytic signal. The absolute phase and modulus of the quotient of the probing and reference analytic signals then give Q and R respectively.

Figure 6(d) shows the baseline phase signals Q_0 ($\psi = 0$) extracted with bandwidth equal to $10f_p$. It is found that the phase can vary in a significant but reproducible way within a given fringe burst. With subtraction of this systematic phase variation, the r.m.s. phase noise in each channel is typically $\leqslant 0.1°$ and appears to be detector noise limited. Figure 6(e) shows the average residual phase obtained after subtraction of Q for two successive wheel scans. Over the 15 channels, the phase standard deviation is 0.08°. Compensating in a similar way for systematic variations in the

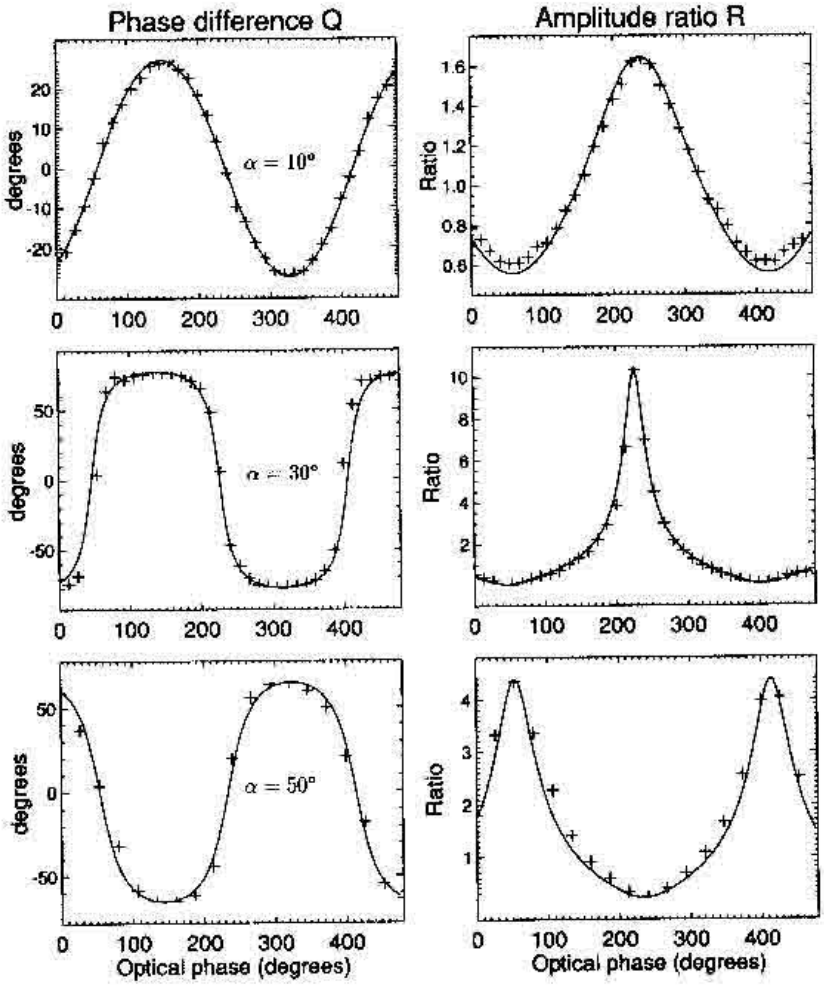

Fig. 7. Plot of phase difference and amplitude ratios for the central channel and ellipse tilt angles $\alpha = 10°$, 30° and 50° (top to bottom). The systematic distortions are due to polarizer leakage.

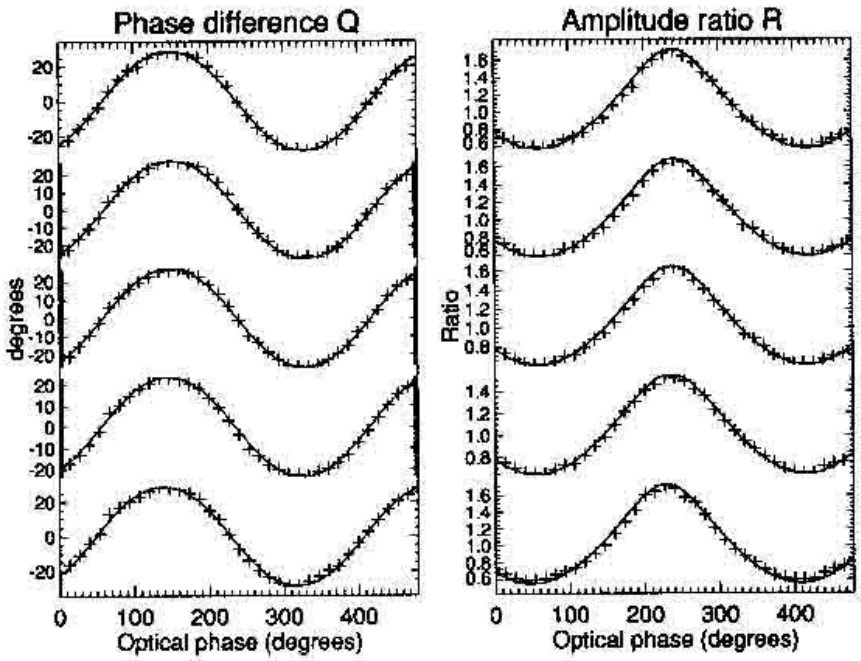

Fig. 8. Plot of phase difference Q and amplitude ratio R for the central five probing beams and for calibration polarizer inclination $\alpha = 10°$.

fringe envelope gives a standard deviation of 0.04 about a mean amplitude ratio of unity. Using equation (21), this corresponds to an uncertainty in the angle 2η of 1.1°, more than an order of magnitude greater than for the direct phase measurement.

The signal-to-noise ratio could be improved by reducing the laser susceptibility to feedback modulation (obviating the need for attenuators) or by using a more powerful laser source. The use of other than corner-cube mounted Schottky detectors could in part reduce the feedback problem.

IV. MEASUREMENTS

For the experiments reported below, a non-zero relative phase shift $Q - Q_0$ is obtained by generating an electric field component orthogonal to E_0 (initially polarized in the x direction). This is done by introducing between the cylindrical return mirror and the grating a calibration polarizer with wires inclined at some angle α. The plane of the polarizer is tilted by 15° to the grating normal to eliminate spurious reflections into the return path. The actual polarizer wire inclination encountered by each beam is obtained from α after allowance for the beam incident angle on the polarizer surface. Because of the double pass of this element, the extinction factor is sufficiently small (see Appendix) to ensure that the beam returned to the grating is approximately linearly polarized orthogonal to the polarizer wires. However, at high angles α, a large fraction of the vertically polarized incident beam is lost so that the signal-to-noise ratio deteriorates and the effects of polarized leakage become more pronounced.

With the above apparatus we have investigated the dependence of the measured phase difference Q and amplitude ratio R on the optical phase ϕ_0 and the ellipse tilt angle ψ. In the former case, this is achieved by varying the PTR separation δ for some fixed inclination α of the calibration polarizer. This contributes to the total phase shift $\phi + \delta + \gamma$ and so is equivalent to varying the birefringence angle ϕ. In the latter case, the optical phase is selected by fixing the PTR separation δ and the return beam polarization varied by changing the wire inclination α of the calibration polarizer. Finally, we note that since the PTR separation is referred to an arbitrary origin, we should write $\delta = \delta' + \delta_0$ where δ' is the absolute phase retardation and δ_0 is the unknown phase origin.

1. Dependence on the birefringence ϕ

The complex grating reflectivity for the various beams is weakly polarization dependent, so that the ideal condition $g = 1$ is not satisfied for all scan beams. In addition, the relative phase shift γ between polarizations parallel and perpendicular to the grating grooves depends on the groove geometry. For the scanning device to operate successfully as a polarimeter in the regime where the birefringence is small (tolerating $g \neq 1$), it is important that the variation in the optical phase ϕ_0 be sufficiently small that the birefringence term in equation (15) remains close to unity for all beams. Fortunately, it is found experimentally that the total spread in ϕ_0 is less than 25°. Indeed, 9 of the 15 beams match to within 5°. This is consistent with the grating calculations noted above. Relative misalignment of the detectors, reflected as differences in the respective fringe envelopes, is possibly a significant source of dispersion of ϕ_0 with channel number.

The unknown optical gain g and phase ϕ_0 as well as the d.c. phase offset Q_0 and relative amplitude scale factor R_0 can be determined by best fitting the ideal functional forms equations (15) and (17) (without regard to polarizer leakage) to experimental measurements of Q and R as a function of the PTR phase δ. Typical phase shifts $Q_0 \sim 10°$ are consistent with expected shifts caused by polarizer leakage [see Appendix and Fig. 6(d)]. Figure 7 shows the measured and best fit ideal curves to the phase difference Q and amplitude ratio R for the central beam (Channel 8) for three settings of the calibration polarizer angle $\alpha = 10°, 30°, 50°$. As noted above, the PTR phase δ is referred to an arbitrary origin. The parameters ϕ_0 and g obtained from best fit of the phase difference variation with δ are used to generate the best fit curves for the amplitude ratio. The quadrature behavior and self-consistency of Q and R is clearly exhibited. The systematic deviations are due to polarizer leakage.

Figure 8 shows the response for the central five polarimeter channels for $\alpha = 10°$. Note the approximate uniformity of ϕ_0 across the array of probe beams and the similarity in the absolute ranges for the phase difference and amplitude ratios.

2. Dependence on the ellipse inclination ψ

Using the curves of Fig. 7 it is possible to adjust the PTR compensator so that the optical phase $\phi_0 \approx 90°$ across all channels. This is also the position where the amplitude ratio is insensitive to the ellipse tilt, the latter appearing as a phase difference $Q \approx 2g\psi$ for small ψ. Figure 9 shows measurements of Q and R vs ellipse tilt ψ for channel 1 (highest Doppler offset). Superimposed are the best fit curves obtained without concern for poarizer leakage. The error bars are 2 standard deviations in length (without compensation for systematic variations). The departure of the ratio

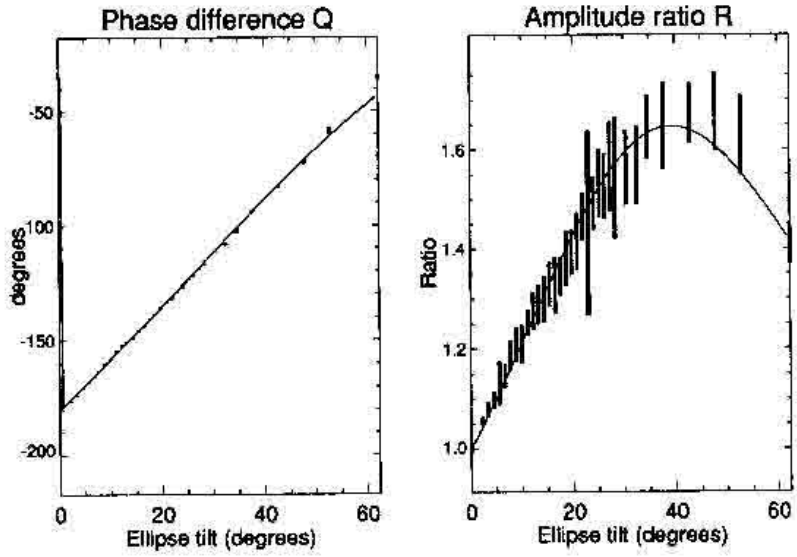

Fig. 9. Measured and ideal best fit to phase difference Q and amplitude ratio R versus ellipse tilt ψ.

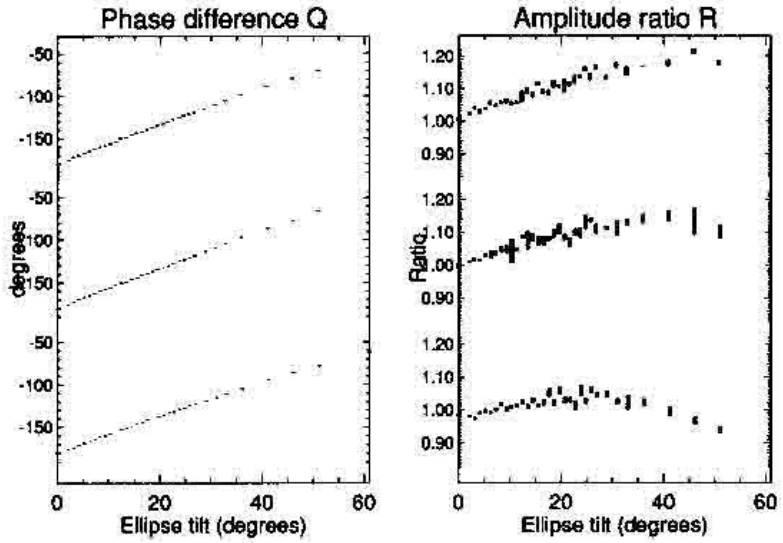

Fig. 10. Measured phase difference Q and amplitude ratio R versus ellipse tilt ψ for the central probing channels. R is insensitive to ψ indicating that the quadrature condition $\phi_0 = \pi/2$ is closely met.

R from unity is attributable to the quadrature condition $\phi_0 = 90°$ being only approximately satisfied for this channel. Nonetheless, the phase Q is seen to depend in an approximately linear fashion on ψ.

Figure 10 shows Q and R again plotted against ψ but for the central channels (7, 8 and 9). The quadrature conditions is here much more closely satisfied, and the amplitude ratios deviate only slightly from unity.

With ϕ_0 set to be near zero, the instrument reverts to the usual intensity measurement technique where, as witnessed in Fig. 11, there is little sensitivity of the phase Q to the ellipse tilt ψ. The position of the phase transition (ideally at $\psi = 45°$—see Fig. 4), however, is sensitive to the optical gain, decreasing to smaller values of ψ for $g > 1$. This is evident in Fig. 11 where the best fit optical gain is $g = 1.23$. All other channels exhibit a comparable response.

V. SUMMARY

A new type of phase-shift heterodyne polarimeter has been described. Experiments that combine the new method with a scanning 15 channel grating in a Michelson configuration have been detailed

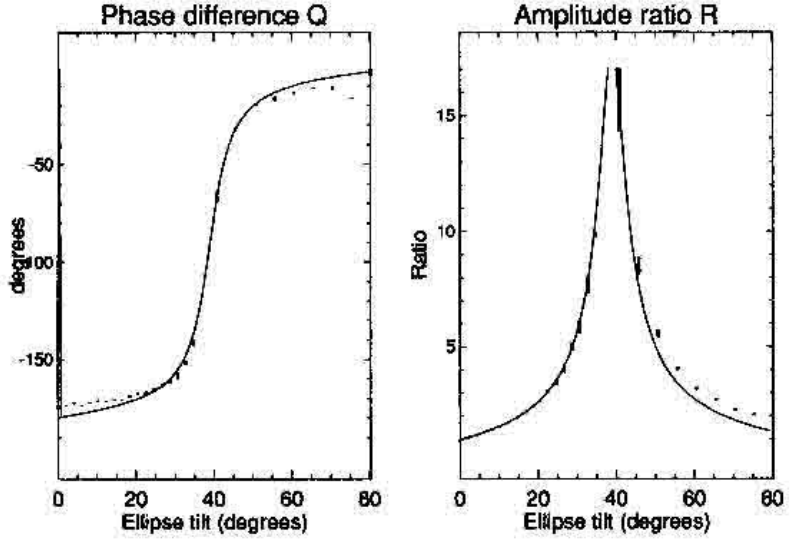

Fig. 11. Measured and ideal best fit curves for the phase difference Q and amplitude ratio R versus ellipse tilt ψ for channel 9. The optical phase is set to $\phi_0 \approx 0$ so that Q is insensitive to ψ.

and agreement with theory demonstrated. Small systematic distortions in the instrument response can be attributed to polarizer leakage. The polarimeter should be capable of attaining phase resolution better than $\sim 0.1^\circ$ with plasma scan rates approaching 1 kHz. Similar experiments using frequency domain multiplexing and with possible extension to infrared wavelengths are underway.

Acknowledgements—The author wishes to thank the Australian Research Council for financial support and S. M. Hamberger for providing the facilities necessary to conduct this research. It is also a pleasure to acknowledge useful discussions with G. B. Warr. This research was in part supported by the Australian Institute of Nuclear Science and Technology.

REFERENCES

1. F. DeMarco and S. E. Segre, *Plasma Phys.* **14,** 245 (1972).
2. A. D. Craig, *Plasma Phys.* **18,** 777 (1976).
3. S. E. Segre, *Plasma Phys.* **20,** 295 (1977).
4. D. Veron, in *Infrared and Millimeter Waves* (Edited by K. Button) Vol. 2, pp. 69–135. Academic Press, New York (1979).
5. F. C. Jobes and D. K. Mansfield, Midplane Faraday rotation: a densitometer for BPX. Technical report, PPPL-2829 (1992).
6. H. Soltwisch and T. Equipe, *Infrared Phys.* **21,** 287 (1981).
7. G. Dodel and W. Kunz, *Infrared Phys.* **18,** 773 (1978).
8. R. Erickson, P. Forman and F. Jahoda, *IEEE Trans. Plasma Sci.* **AP-17,** 275 (1984).
9. A. B. Carlson, *Communication Systems*. McGraw-Hill, Singapore (1986).
10. T. Fukuda, S. Goto, T. Ishimura and H. Ito, *Int. J. Infrared Millimeter Waves* **5,** 1039 (1984).
11. W. Kunz and G. Dodel, *Plasma Phys.* **20,** 171 (1978).
12. B. W. Rice, Fifteen chord FIR polarimetry system on MTX. In *Press. Rev. Sci. Instrum.* (1992).
13. J. Howard, *Rev. Sci. Instrum.* **61,** 1086 (1990).
14. J. Howard, G. B. Warr and P. Dodds, *Rev. Sci. Instrum.* **63,** 4965 (1992).
15. J. Howard, W. Peebles and N. Luhmann Jr, *Int. J. Infrared Millimeter Waves* **7,** 1591 (1986).
16. H. Ikuno and K. Yasuura, *IEEE Trans. Antennas Propagat.* **AP-21,** 657 (1973).
17. K. D. Möller and W. G. Rothschild, *Far-Infrared Spectroscopy*. Wiley, New York (1971).

APPENDIX

In the coordinate system aligned with the polarizer wires (assumed lossless), the reflected and transmitted field amplitudes, expressed in terms of the components parallel and perpendicular to the wires, are

$$\mathbf{E}_R = \mathbf{P}_0^R \begin{pmatrix} E_\parallel \\ E_\perp \end{pmatrix} \quad \mathbf{E}_T = \mathbf{P}_0^T \begin{pmatrix} E_\parallel \\ E_\perp \end{pmatrix}. \tag{A1}$$

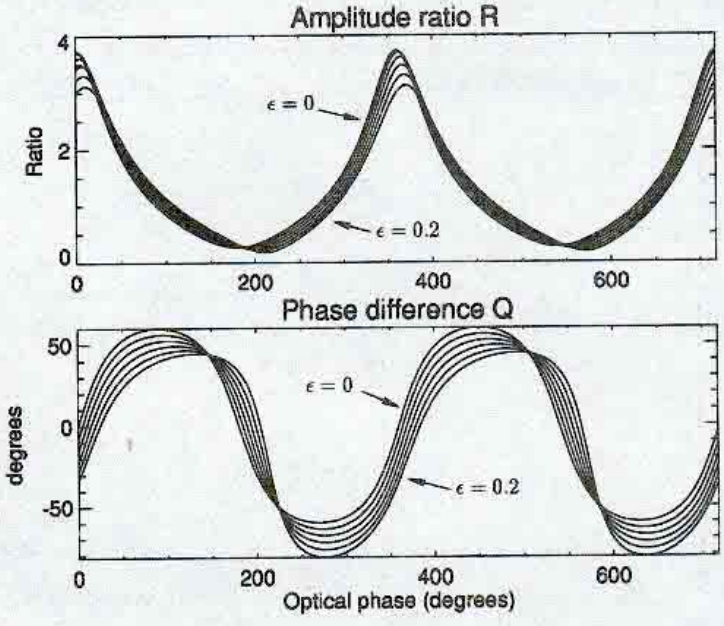

Fig. A1. Dependence of the amplitude ratio R and phase difference Q on the optical phase ϕ_0 for fixed ellipse tilt angle $\psi = 60^\circ$ and for various values of the polarizer extinction ratio $\epsilon = 0(0.04)\ 0.2$.

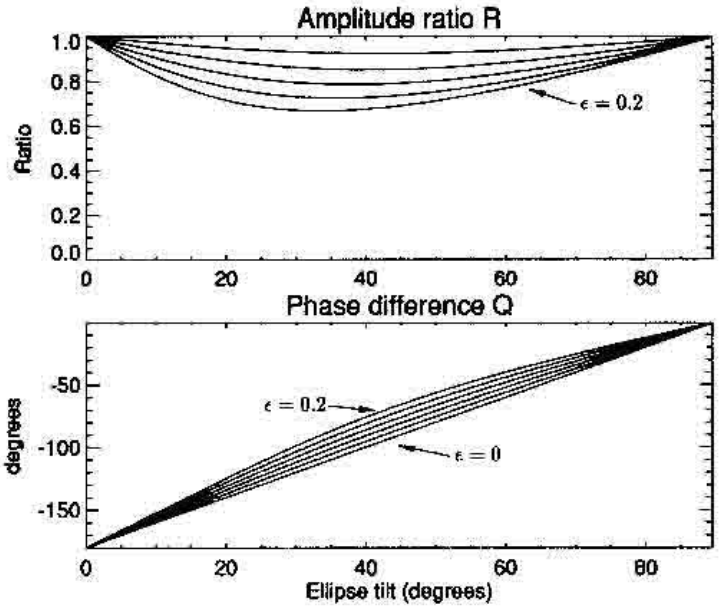

Fig. A2. Dependence of the amplitude ratio R and phase difference Q on the ellipse tilt ψ for fixed $\phi_0 = 90°$ and for various values of the polarizer extinction ratio $\epsilon = 0(0.04)0.2$.

The reflection and transmission matrices are given by

$$\mathbf{P}_0^{\mathrm{R}} = \begin{pmatrix} \rho_{\parallel} \exp j\phi_{\parallel}^{\mathrm{R}} & 0 \\ 0 & \rho_{\perp} \exp j\phi_{\perp}^{\mathrm{R}} \end{pmatrix} \quad \mathbf{P}_0^{\mathrm{T}} = \begin{pmatrix} \tau_{\parallel} \exp j\phi_{\parallel}^{\mathrm{T}} & 0 \\ 0 & \tau_{\perp} \exp j\phi_{\perp}^{\mathrm{T}} \end{pmatrix} \tag{A2}$$

where the following relationships hold:[17]

$$\begin{aligned} \phi_{\parallel}^{\mathrm{R}} &= \pi - \tan^{-1}(\tau_{\parallel}/\rho_{\parallel}) \quad \phi_{\parallel}^{\mathrm{T}} = \tan^{-1}(\rho_{\parallel}/\tau_{\parallel}) \\ \phi_{\perp}^{\mathrm{R}} &= \pi + \tan^{-1}(\tau_{\perp}/\tau_{\perp}) \quad \phi_{\perp}^{\mathrm{T}} = -\tan^{-1}(\rho_{\perp}/\tau_{\perp}) \end{aligned} \tag{A3}$$

and

$$\rho_{\parallel} = \tau_{\perp} \quad \rho_{\perp} = \tau_{\parallel} \quad \tau^2 + \rho^2 = 1. \tag{A4}$$

If the wires are oriented at angle α with respect to the x axis the polarizer matrix in transmission is given by

$$\begin{aligned} \mathbf{P}_{\alpha}^{\mathrm{T}} &= \mathbf{R}_{\alpha}^{-1} \mathbf{P}_0^{\mathrm{T}} \mathbf{R}_{\alpha} \\ &= \frac{\exp(-j\zeta)}{(1+\epsilon^2)^{1/2}} \begin{pmatrix} \sin^2\alpha + j\epsilon\cos^2\alpha & -\sin\alpha\cos\alpha(1-j\epsilon) \\ -\sin\alpha\cos\alpha(1-j\epsilon) & \cos^2\alpha + j\epsilon\sin^2\alpha \end{pmatrix} \end{aligned} \tag{A5}$$

where $\epsilon = \tau_{\parallel}/\tau_{\parallel}$ is the extinction ratio and $\zeta = \tan^{-1}\epsilon$. In reflection, it can shown that the polarizer properties are described by equation (10).

In terms of the wire separation w and radius a, the extinction ratio is given by[17]

$$\epsilon = \frac{2w}{\lambda_0} \ln \frac{w}{2\pi a}. \tag{A6}$$

For $w = 25\,\mu$m and $2a = 12.5\,\mu$m we obtain $\epsilon \approx 0.07$ compared with a measured value $\epsilon = 0.12 \pm 0.2$.

Taking account of the polarizer leakage and retaining terms only to first order in ϵ, the measured phase difference becomes

$$\tan Q_1 = \tan Q \begin{pmatrix} 1 - 2\epsilon\cot(\phi + \delta + \gamma) \\ 1 + 2\epsilon\sin\delta \end{pmatrix}. \tag{A7}$$

By setting the probe beam polarization so that η and ϕ are known, the fit of this function to experimental measurements of Q_1 vs δ requires estimation of the unknown parameters ϵ, g, and γ. The correction term results in a small d.c. offset in the total excursion of Q_1 with δ while the positions of the zero-crossings are given by $\tan(\phi + \phi_0) = 2\epsilon$. For the fits shown in Section IV(1) we have simply removed the d.c. offset and fitted the functional form given by equation (15) to the data.

The dependence of Q and R on ϕ_0 for polarizer extinction ratios $\epsilon = 0.0\ (0.04)\ 0.12$ and for ellipse tile $\psi = 60°$ is shown in Fig. A1. Note the distortion, phase shift and change in d.c. level Q_0 for the phase difference Q. The effects of polarizer leakage on the variation of Q and R with ψ (at $\phi_0 = 90°$) are shown in Fig. A2. Though even small leakages can compromise the linearity of Q with ψ, the effects are more sensitively felt by the signal ratio R. The leakage-induced distortions can be easily accounted by suitable calibration of the polarimeter. Alternatively, the effects can be reduced to insignificant levels by constructing more efficient polarizers or by cascading the leaky polarizers.